Angular Distribution of Visible and Near IR Radiation Reflected from CO_2 Cryodeposits

A. M. Smith,* K. E. Tempelmeyer,† P. R. Müller,‡ and B. E. Wood§
ARO Inc., Arnold Air Force Station, Tenn.

The effect of CO_2 cryodeposits on the angular distribution of visible and near IR radiation reflected from polished copper and black epoxy paint surfaces is investigated experimentally. It is found that the presence of CO_2 cryodeposit on a surface causes the incident radiation to be reflected more diffusely. Also, off-specular peaks are observed in the directional distributions of reflected radiation, and the angular location of these peaks relative to the specular direction is found to be a function of deposit thickness and deposition rate as well as irradiation incidence angle. In addition, the experimental results indicate that CO_2 cryodeposits scatter more in the backward direction than in the forward. Finally, "scattering interference" patterns are seen in the angular distribution measurements for the cryodeposits formed on polished copper. These patterns are a result of interference generated by scattering at the vacuum-cryodeposit interface and they can be used to measure the thickness of thin layers of CO_2 cryodeposit.

Introduction

In most thermal-vacuum space simulation chambers the test vehicle is surrounded by panels cooled to near 77°K by LN_2. These surfaces are normally painted black to minimize the reflection of incident radiation from the solar simulator. However, as CO_2 and H_2O cryodeposits form on the panels because of cryopumping, the reflective characteristics of the black surfaces change and the test vehicle thermal balance will be altered. To properly interpret the resulting thermal balance test data, it is necessary to determine how cryodeposits affect the visible and near IR reflection properties of these panels. Reference 1 reports detailed angular-hemispherical reflectance measurements which have been obtained for CO_2 and H_2O cryodeposits on copper and black painted cryosurfaces. The objective of this paper is to present extensive in situ measurements of the angular distribution of visible and near IR radiation reflected from thin CO_2 cryodeposits formed on polished copper and black epoxy paint substrates.

Previous angular distribution measurements which have been reported for CO_2 cryodeposits on copper and black painted surfaces[2] were of a preliminary nature. In the work presented here, detailed angular distribution data are given for CO_2 deposits of thicknesses ranging from 2.25 to 270 μ. These results are useful in determining how CO_2 cryodeposits affect the angular distribution of solar simulator radiation reflected from space chamber cryopanels. They also contribute additional information on the basic reflection properties of CO_2 cryodeposits formed on opaque substrates. In particular, one group of these results reports the first observation of a new and important phenomenon which occurs for solid films of CO_2 deposited on a specularly reflecting substrate. This phenomenon has been termed "scattering interference" and it may have application to the in situ optical measurement of cryodeposit thickness in space simulation chambers.

Presented as Paper 69-63 at the AIAA 7th Aerospace Sciences Meeting, New York, January 20–22, 1969; submitted February 11, 1969; revision received June 12, 1969. This work was sponsored by the Arnold Engineering Development Center, Air Force Systems Command, under Contract F40600-69-C-0001 with ARO Inc.

* Supervisor, Thermal Radiation Section, Aerospace Environmental Facility; also Associate Professor of Aerospace Engineering, University of Tennessee Space Institute, Tullahoma, Tenn. Member AIAA.

† Manager, Research Branch, Aerospace Environmental Facility. Associate Fellow AIAA.

‡ Research Assistant, Aerospace Environmental Facility and University of Tennessee Space Institute, Tullahoma, Tenn.

§ Project Engineer, Thermal Radiation Section, Aerospace Environmental Facility. Associate Fellow AIAA.

Experimental Apparatus

The experiments were conducted in a spherical vacuum chamber which had an LN_2-cooled copper cryosurface located at its center as shown in Fig. 1. To minimize internal reflections, all interior surfaces of the vacuum chamber except one face of the cryosurface were coated with a flat black paint. This face was polished to an rms surface roughness of less than 0.01 μ. It was used as the test surface and was either coated with black epoxy paint or was just the bare polished copper. The test surface could be rotated to any desired polar angle with respect to the incident beam of collimated radiation and its position set to $\pm 0.5°$. As shown in the schematic, the collimated irradiance was obtained from a 1600-w xenon arc lamp by means of a condensing lens system and a collimating tube built into the vacuum chamber port. Both the interior and exterior of the collimating tube were blackened. A xenon lamp was used for the visible and near IR radiation source because state-of-the-art solar simulators commonly employ high-power xenon arc lamps as radiation sources. Monochromatic irradiance could be obtained by inserting interference filters between the condensing lens system and the quartz lens on the chamber port. All measurements of reflected radiation were made using a silicon solar cell detector mounted on a remotely rotatable arm (see Fig. 1). Carbon dioxide gas of 99.8% purity could be introduced into the vacuum chamber at three different flow rates by means of a calibrated leak system.

Procedure

The angular distribution of the reflected radiation leaving the CO_2 deposit was determined by the biangular method illustrated in Fig. 2. In this technique, the cryodeposit is irradiated by a collimated beam of radiant flux $E_i(\psi,\zeta)$ in a direction defined by the polar incidence angle ψ and the azimuthal incidence angle of $\zeta = 180°$. Reflected radiant flux

leaving the cryodeposit of thickness τ through a solid angle $\Delta\omega_r$ in the direction defined by the polar reflection angle θ and the azimuthal reflection angle φ is denoted as $E_r(\psi,\zeta;\ \theta,\varphi;\ \tau)$. The detector was so arranged in the chamber that its rotation at constant angular velocity about the vertical centerline of the surface mapped the angular distribution of the reflected radiant flux in the plane of incidence, $E_r(\psi,\ 180°;\ \theta,\varphi;\ \tau)$, for reflection angles of $\varphi = 0°$, $0° \leq \theta \leq 90°$ and $\varphi = 180°$, $0° \leq \theta \leq 60°$.

Angular Distribution Measurements

After the vacuum chamber had been evacuated to a pressure of about 1×10^{-6} torr and valved off from the pumping system, the xenon lamp was turned on and the test surface rotated to the desired polar incidence angle ψ. Then, with the test surface still at 300°K, the detector was rotated about it in the plane of incidence and a reference trace of the angular distribution of the reflected radiant flux was made for the surface when no cryodeposit was present ($\tau = 0$). The test surface was rotated to other values of ψ and the mapping procedure repeated. Next, the cryosurface was cooled to 77°K and the vacuum chamber back-filled with helium to achieve the desired deposition pressure P. Prior to forming the cryodeposit, the polar incidence angle ψ of the irradiance was set at some particular value, the detector was positioned in the direction of specular reflection ($\theta = \psi$, $\varphi = 0°$), and a filter of 0.9 μ wavelength was inserted into the radiation beam. Then, a cryodeposit layer of a given thickness was formed on the test surface by flowing CO_2 gas into the chamber at a constant rate for a specified time t. The reflected radiation leaving the cryodeposit in the specular direction was monitored continuously by the detector as the deposit formed. After the gas flow was stopped, the filter was removed from the radiation beam and the angular distribution of the reflected visible and near IR radiant flux was recorded for various values of ψ. Then, CO_2 was again added to the chamber forming another cryodeposit layer on top of the first and the previous radiation measurements were repeated. This procedure was continued and measurements made for each resulting cryodeposit thickness.

In Situ Measurement of Deposition Rate and Cryodeposit Thickness

The deposition rate $\dot{\tau}$ for each cryodeposit was measured in situ by continuously monitoring the 0.9 μ wavelength radiation reflected in the specular direction as the deposit formed on the test surface.[3,4] Rays which are 1) specularly reflected from the vacuum-cryodeposit interface and 2) specularly reflected from the cryodeposit-substrate interface are alternately in and out of phase with each other as the deposit thickness increases and a detector located at the specular reflection angle $\theta = \psi$, $\varphi = 0°$ experiences a varying signal such as shown in Fig. 3. The data given in Fig. 3 are for the black epoxy paint substrate but the same type of pattern also occurs for the polished copper substrate. With total irradiation, similar patterns are observed for

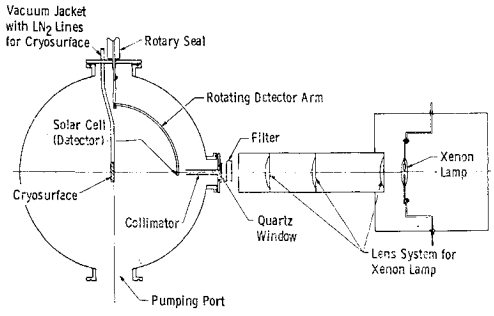

Fig. 1 Schematic of experimental apparatus.

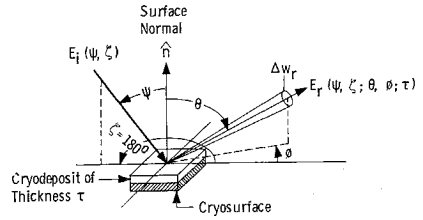

Fig. 2 Spatial coordinates for incident and reflected radiant fluxes.

deposit thicknesses up to 2 μ but for thicker deposits there exists no interference such as found with monochromatic irradiation and portrayed in Fig. 3.[5]

From the well-known condition for existence of constructive interference between the aforementioned specularly reflected rays,[6]

$$\tau = q\lambda/[2n(1 - \sin^2\psi/n^2)^{1/2}],\ q = 1, 2, 3, \ldots \quad (1)$$

it is apparent that the change in cryodeposit thickness $\Delta\tau$ between adjacent maxima in Fig. 3 is given by

$$\Delta\tau = \Delta q\lambda/[2n(1 - \sin^2\psi/n^2)^{1/2}] \quad (2)$$

where $\Delta q \equiv 1$ and n is the index of refraction of the cryodeposit at the wavelength λ of the incident monochromatic radiation. Since the gas addition rate to the vacuum chamber is invariant with time, the cryodeposit forms at a constant deposition rate, or $\dot{\tau} \equiv d\tau/dt = \text{const}$. This is demonstrated by the essentially equal spacing between adjacent maxima or minima in the results of Fig. 3. Hence, from Eq. (2), the relation for the constant deposition rate is

$$\dot{\tau} = \Delta\tau/\Delta t = \lambda/[2n\Delta t(1 - \sin^2\psi/n^2)^{1/2}] \quad (3)$$

where Δt is the time interval between adjacent maxima and can be obtained from experimental data such as that shown in Fig. 3. Thus, $\dot{\tau}$ can be expressed in terms of measurable quantities.[4]

The cryodeposit thickness was determined in two ways. For thin deposits where the ordinary thin-film interference phenomenon is observed, Eq. (1) was used to calculate the thickness with $q = 1$ corresponding to the first maxima, $q = 2$ to the second maxima, etc., in the experimental data (see Fig. 3). This technique is applicable up to deposit thicknesses of about 20 μ. For thicker deposits, the thickness was determined by taking the product of the constant deposition rate $\dot{\tau}$ and the measured deposition time t.

Results and Discussion

Some results of the angular distribution measurements described in the previous section are given in Figs.4 and 5. The data shown are for CO_2 deposits formed at a deposition

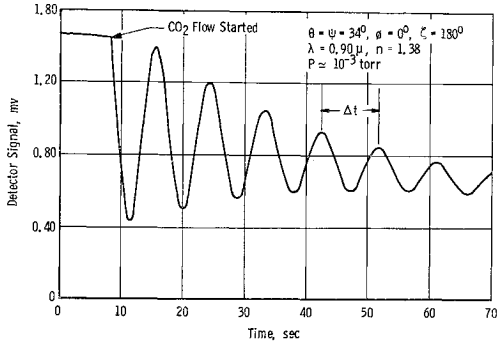

Fig. 3 Thin-film interference pattern obtained at the specular reflection angle when CO_2 cryodeposit is being formed on a black epoxy paint substrate at a deposition rate of 2.25 μ/min.

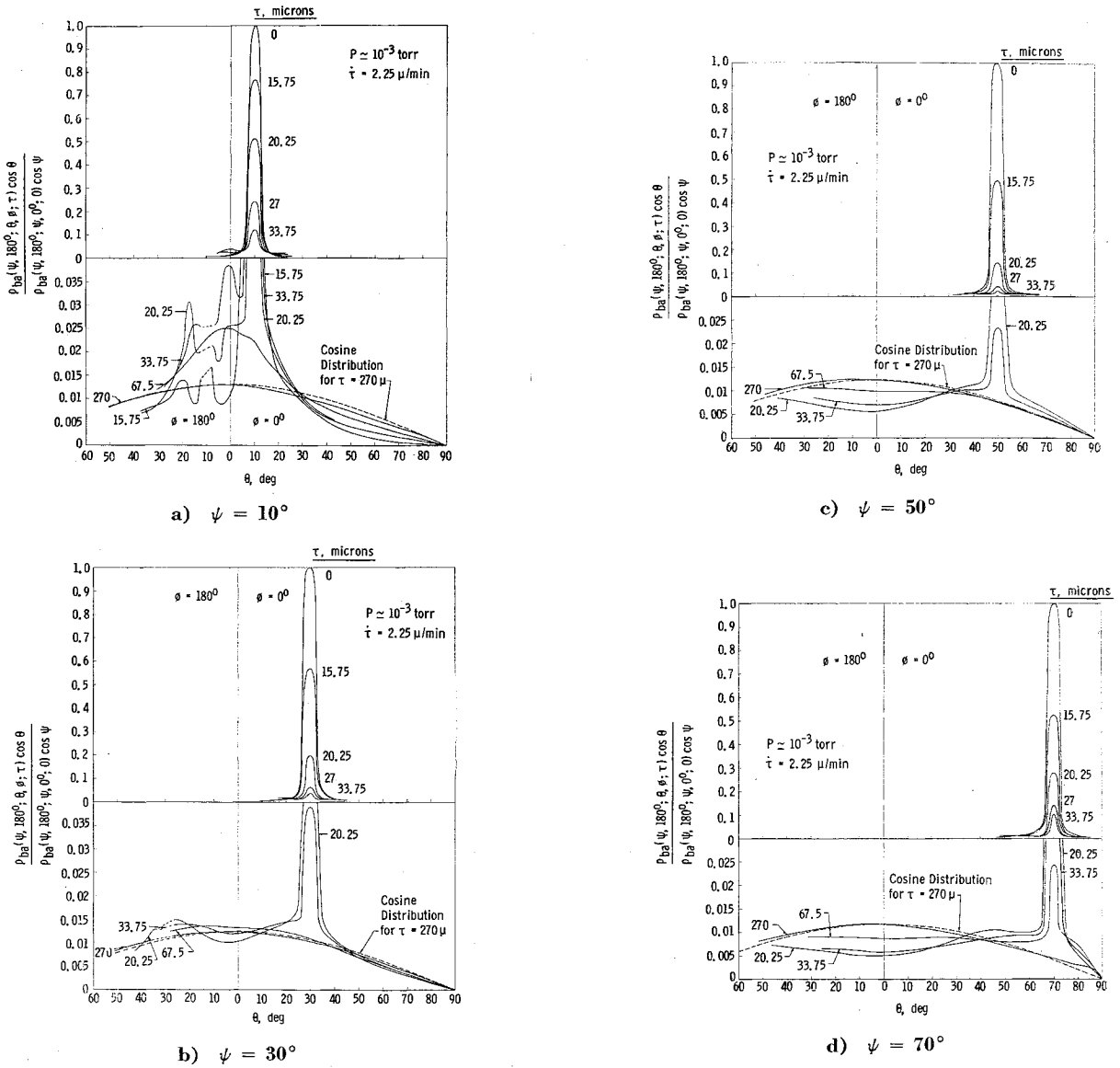

Fig. 4 Angular distribution of visible and near IR radiant flux reflected from CO_2 cryodeposits formed on a polished copper substrate.

pressure of approximately 10^{-3} torr and a deposition rate of 2.25 μ/min. In Figs. 4 and 5, the angular distribution measurements made in the plane of incidence ($\zeta = 180°$, $\varphi = 180°$ and 0°) are presented in terms of a normalized ratio of reflected fluxes $E_r(\psi,180°;\ \theta,\varphi;\ \tau)/E_r(\psi,180°;\ \psi,0°;\ 0)$ where, for irradiation of the surface in the direction $\psi,\zeta = 180°$, E_r $(\psi,180°;\ \theta,\varphi;\ \tau)$ represents the radiant flux reflected in the direction θ, φ when a cryodeposit of thickness τ is present on the substrate and $E_r(\psi,180°;\ \psi,0°;\ 0)$ represents the radiant flux reflected in the specular direction $\theta = \psi$, $\varphi = 0°$ when no cryodeposit is present ($\tau = 0$). As indicated on the ordinate scale labels of the figures, this ratio of reflected radiant fluxes can also be expressed as[7] $\rho_{ba}(\psi,180°;\ \theta,\varphi;\ \tau)\cos\theta/\rho_{ba}(\psi,180°;\ \psi,0°;\ 0)\cos\psi$ where $\rho_{ba}(\psi,\zeta;\ \theta,\varphi;\ \tau)$, the bidirectional reflectance, is defined as $\pi I_r(\psi,\zeta;\ \theta,\varphi;\ \tau)/E_i(\psi,\zeta)$ with $I_r(\psi,\zeta;\ \theta,\varphi;\ \tau)$ being the reflected radiant intensity associated with the reflected radiant flux $E_r(\psi,\zeta;\ \theta,\varphi;\ \tau)$. It should be noted that the distribution curves in Figs. 4 and 5 are interrupted by either dashes or dots in the region $\varphi = 180°$, $\theta \simeq \psi$. This indicates that no distribution measurements were made in this direction because as the detector arm passed the angle $\theta \simeq \psi(\varphi = 180°)$, it blocked off the incident beam of radiation and the detector output was zero.

Angular Distributions of Reflected Radiant Flux

Figure 4 presents the angular distributions of visible and near IR radiant flux reflected from CO_2 cryodeposits on a polished copper substrate for polar incidence angles of 10°, 30°, 50°, and 70° and cryodeposit thicknesses ranging from 15.75 μ to 270 μ. Note that distribution values of equal or less than 0.04 are displayed on a greatly increased scale in the lower segment of each graph. It is seen in Fig. 4 that the presence of CO_2 cryodeposits on a polished copper substrate, which itself is a highly specular reflector, causes the radiant flux reflected in the specular direction $\theta = \psi$, $\varphi = 0°$ to decrease rapidly with increasing cryodeposit thickness. At a deposit thickness of 67.5 μ, the specular peak in the reflected flux has almost disappeared, except for a polar incidence angle of 70°. This rapid decrease and eventual disappearance of the specular peak as the cryodeposit thickens is accompanied by an increase in the radiant flux reflected in nonspecular directions until for a deposit thickness of 270 μ the distribution of reflected flux is essentially diffuse. Such behavior can be explained by noting that due to both surface and internal scattering by the cryodeposit, the incident visible and near IR radiation will be reflected in directions other than just the specular direction. At first, when the deposit

is relatively thin, the surface scattering will likely predominate. However, as the deposit thickens, the internal scattering becomes increasingly significant until it has a much greater effect on the reflected flux distribution than does the surface scattering thereby causing the angular distribution of the reflected flux to approach a diffuse distribution. Two other important phenomena are observed in the angular distributions presented in Fig. 4. The first is the existence, as seen in Fig. 4a, of several unexpected peaks in the distribution of the radiant flux reflected from relatively thin deposits of $\tau = 15.75$, 20.25, and 33.75 μ. These peaks have been termed "scattering interference" peaks for reasons which will be discussed below. The second important phenomenon observed in the distributions of Fig. 4 is that, for deposits of thickness $\tau = 20.25$, 33.75, and 67.5 μ, the radiant flux reflected into directions lying within the quadrant of incidence ($\varphi = 180°$, $\theta > 0°$) is generally larger than the flux reflected in the direction normal to the surface $\theta = 0°$ (Figs. 4b, 4c, and 4d). This gives the impression that CO_2 cryodeposits scatter significantly in the backward direction.

Figure 5 presents the angular distributions of visible and near IR radiant flux reflected from CO_2 cryodeposits formed on a black epoxy paint substrate whose normal reflectance was 5%. The results shown are for polar incidence angles of 10°, 30°, 50°, and 70° and deposit thicknesses ranging from 2.25 to 270 μ.¶ It is noted that, for deposit thicknesses up to 15.75 μ, the decrease in the normalized flux reflected in the specular direction is greater than was observed for thin ($\tau \lesssim 20$ μ) CO_2 deposits formed on polished copper. This is due to the increased surface scattering which results from the vacuum-cryodeposit interface being rougher for the thin CO_2 deposits formed on the black paint. At deposit thicknesses of about 67.5 μ and above, the specular peak in the reflected flux has essentially disappeared for the lower incidence angles but for an incidence angle of 70° a small peak in the reflected flux still exists near the specular direction. Just as for the CO_2 deposits formed on the polished copper substrate, this diminishing of the specular peak and the accompanying increase in the radiant flux reflected in other directions is due to surface and internal scattering. As the deposit thickens, the internal scattering becomes more significant. This is vividly illustrated in Figs. 5a and 5b by noting that an increase in the deposit thickness from 67.5 to 270 μ causes the amount of flux reflected in most all directions ($\theta \neq 90°$) to increase by a factor of about ten. It is also observed in Fig. 5 that for all angles of incidence the distribution of the radiant flux reflected from a 270 μ thick deposit approximates a diffuse distribution. However, the radiant flux reflected into directions lying within the quadrant of incidence $\varphi = 180°$, $\theta > 0°$ is significantly larger than the flux reflected into directions lying within the quadrant of specular reflection $\varphi = 0°$, $\theta > 0°$. This indicates that CO_2 cryodeposits scatter more in the backward direction than in the forward.

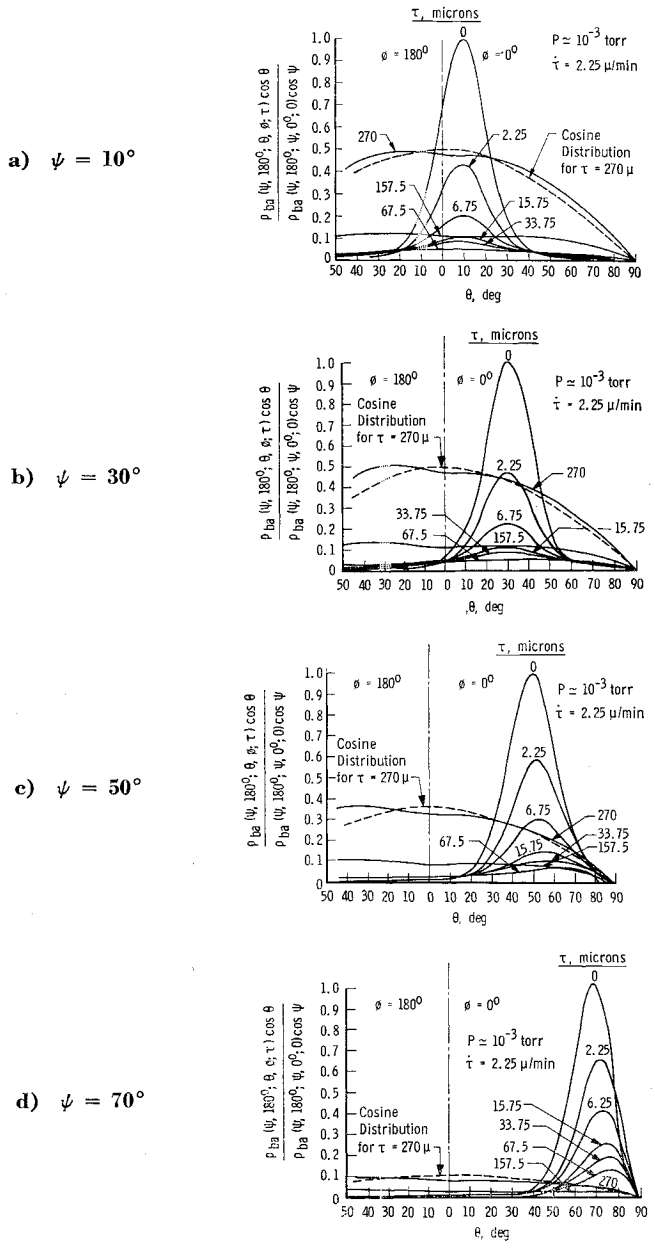

Fig. 5 Angular distribution of visible and near IR radiant flux reflected from CO_2 cryodeposits formed on a black epoxy paint substrate.

Off-Specular Peaks in the Reflected Flux Distributions

Another phenomenon observed for CO_2 cryodeposits on a black epoxy paint substrate is that the maxima in the reflected flux distributions do not occur in the specular direction when the polar incidence angles are large. It is seen in Figs. 5c and 5d that these off-specular peaks occur at polar reflection angles $\theta_p(\varphi = 0°)$ which are greater than the specular reflection angle $\theta = \psi(\varphi = 0°)$. In Ref. 5, it is found that the difference between the angular locations of the off-specular peak and the specular direction $\theta_p - \psi$ is a function of the irradiance incidence angle, $\psi(\zeta = 180°)$. For polar incidence angles equal or less than 40°, the peaks in the reflected flux distributions occur in the specular direction and $\theta_p - \psi$ equals zero. However, for polar incidence angles from 50° to 70°, $\theta_p - \psi$ is greater than zero. This behavior of $\theta_p - \psi$ with angle of incidence is consistent with the trends reported by Torrance and Sparrow[8] for the off-specular peak phenomenon on mechanically roughened surfaces. It is noted in Figs. 5c and 5d that the angular displacements of the off-specular peaks relative to the specular direction also depend upon the thickness of the deposit. This is better illustrated in Fig. 6 where $\theta_p - \psi$ for an incidence angle of 70° is displayed as a function of deposit thickness up to 75 μ with deposition rate taken as a parameter. It is seen that for a CO_2 cryodeposit formed at a deposition rate of 2.25 μ/min, the angular displacement of the off-specular peak relative to the specular direction increases from 0° to 10° as the deposit thickness increases up to 67 μ. Most of this change in $\theta_p - \psi$ occurs before the deposit reaches a thickness of 20 μ. It

¶ Unlike polished copper, the radiant flux reflected from the bare black paint substrate in the specular direction increases significantly for the higher angles of incidence.[5] Therefore, in Fig. 5, no attempt should be made to compare the relative heights of the distribution curves for a given deposit thickness at different angles of incidence since the normalizing factor for each incidence angle may be different.

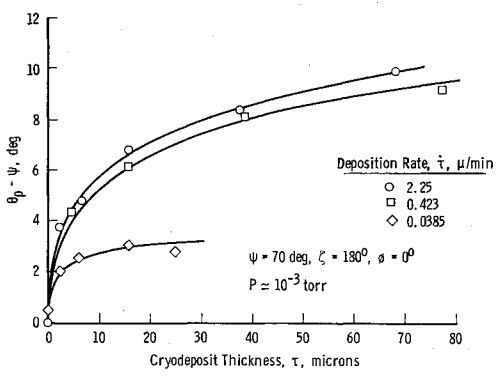

Fig. 6 Difference between the angular locations of the off-specular peak and the specular direction for visible and near IR radiant flux reflected from CO_2 cryodeposits formed at various deposition rates on a black epoxy paint substrate.

is also seen in Fig. 6 that the value of $\theta_p - \psi$ is essentially the same for deposits formed at the two higher deposition rates of 2.25 and 0.423 μ/min. However, the magnitude of $\theta_p - \psi$ is much smaller for deposits formed at the lowest deposition rate 0.0385 μ/min and is relatively constant at a value of approximately 3° for deposit thicknesses equal or greater than 5 μ. This indicates that the angular displacement of the off-specular peak from the specular direction also depends upon the rate at which the deposit was formed.

The occurrence of off-specular peaks for CO_2 cryodeposits formed on a black epoxy paint substrate, as seen in Fig. 5, and the dependence of their angular location on deposit thickness and deposition rate, as shown in Fig. 6, can possibly be explained as follows. It will be hypothesized that the characteristic roughness of the surface of the black paint substrate was not much less than the characteristic wavelength of the incident radiation (0.9 μ ±0.1) and the top surface of the cryodeposit formed on this substrate was even rougher so that its surface roughness was comparable to or greater than the characteristic wavelength of the incident radiation. If this hypothesis is correct, then based on the results of Ref. 8, the peak in the reflected flux should shift to a polar reflection angle greater than the specular reflection angle. The increase in the angular displacement of the off-specular peak as the deposit thickened then indicates that the roughness of the deposit surface increased with deposit thickness until possibly reaching some limiting value. This limiting value of the surface roughness of the deposit would likely be a function of deposition rate with the deposit surface perhaps being much smoother for the low deposition rates. If such is the case, then the angular displacement of the off-specular peak would be much less, as is observed in Fig. 6 for the lowest deposition rate of 0.0385 μ/min.

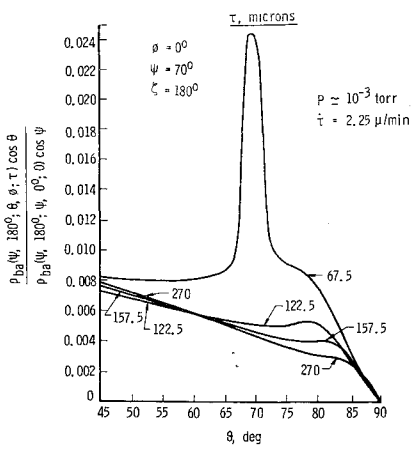

Fig. 7 Off-specular peaks in the visible and near IR reflected flux distributions for CO_2 cryodeposits formed on polished copper, ψ = 70°.

The above hypothesis can also be used to explain why no off-specular peaks were observed in the distribution results for CO_2 cryodeposits on polished copper until the deposit thickness approached 122.5 μ (see Fig. 7). In this case, the rms surface roughness of the substrate (0.01 μ) was much less than the characteristic wavelength of the incident radiation. Hence, the top surface of a thin deposit formed on the polished copper, while likely to be rougher than the substrate surface, would still have a surface roughness which was considerably less than the characteristic wavelength of the incident radiation and no off-specular peak should occur. However, as the deposit thickens, the surface roughness of the deposit will increase with thickness and eventually reach a value comparable to or greater than the characteristic wavelength of the incident radiation. Thus, for some deposit thickness and incidence angle, it would be possible, as seen in Fig. 7, to observe off-specular peaks in the distribution results for CO_2 cryodeposits on polished copper.

Scattering Interference Patterns

As can be seen in the incidence quadrant of Fig. 4a, scattering interference peaks occur in the angular distributions of visible and near IR radiant flux reflected from relatively thin CO_2 cryodeposits formed on polished copper. When monochromatic irradiance of 0.9 μ wavelength is employed, the interference peaks are much more numerous and better

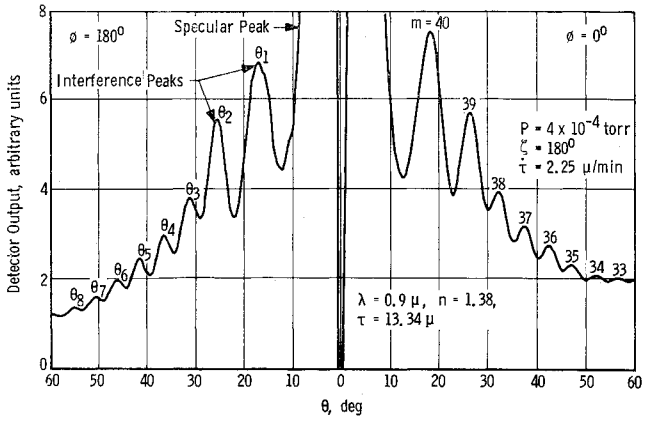

a) ψ = 0°

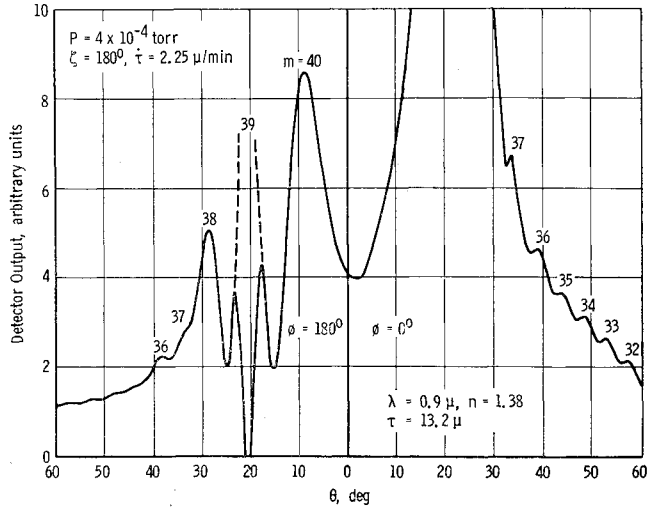

b) ψ = 21.5°

Fig. 8 Scattering interference patterns obtained for a 13.37-μ thick CO_2 cryodeposit on a polished copper substrate, λ = 0.9 μ.

defined, as seen in Fig. 8. This figure shows, for polar incidence angles of 0° and 21.5°, the unnormalized angular distribution measurements for a CO_2 cryodeposit of 13.37 μ thickness. The deposit thickness, which is given in the figure caption, was determined from Eq. (1) using the technique described previously. In Fig. 8a, which is for $\psi = 0°$, interference peaks are seen to occur at polar reflection angles $\theta_j, j = 1, 2, 3, \ldots, 8$ for both $\varphi = 180°$ and $\varphi = 0°$. Thus, the polar angular locations of the interference peaks appear to be symmetrical about $\theta = 0°$. The base of the specular peak is also seen in Fig. 8a as is the zero detector output occurring at $\theta \simeq \psi = 0°$ due to detector arm blockage of the incident beam of radiation. Figure 8b shows the scattering interference pattern observed when the polar incidence angle of the irradiance is 21.5°. It is noted that, in general, the interference peaks are not as well resolved as for an incidence angle of 0°. However, three quite strong peaks occur in the $\theta < 30°$ region of the quadrant of incidence with the angular location θ_2, $\varphi = 180°$ of the center peak lying quite near the direction of incidence $\psi = 21.5°$, $\zeta = 180°$. Most of this peak is, of course, not seen because the detector output is zero at $\theta \simeq \psi$, $\varphi = 180°$ due to reasons given previously. The base of the specular peak is also observed in Fig. 8b and is centered about $\theta = 21.5°$, $\varphi = 0°$.

Theoretical Model for the Scattering Interference Patterns

Interference patterns such as those shown in Fig. 8 have been observed for CO_2 cryodeposits of thicknesses ranging from 5 to 100 μ. These patterns have been termed scattering interference patterns because they are thought to result from interference which is generated by scattering at the vacuum-cryodeposit interface. The manner in which this interference occurs can be explained by the interface scattering model shown in Fig. 9. In this model, the incident beam of collimated monochromatic radiation strikes the cryodeposit surface at point A at an angle ψ from the normal. A portion of this beam is assumed to be directly reflected and scattered by the vacuum-cryodeposit interface into an r family of rays. The distribution of rays in the r family is unknown. However, it is assumed to have a specular component at $\theta = \psi$. In addition, the wavefronts corresponding to the reflected rays are assumed to undergo a 180° phase shift since the refractive index of the cryodeposit is greater than that of the vacuum.[9]

Radiation which is transmitted through the vacuum-cryodeposit interface is assumed to be scattered into, say the t family of rays. Again, the distribution of rays in the t family is not known, but it is made up of a refracted component, ray t_s, and an infinite number of scattered t rays. Since the deposit is relatively thin, internal scattering and absorption are assumed to be negligible, and an arbitrary scattered t ray t_j will be incident on the substrate at point B at an angle β_j. This ray is specularly reflected with a 180° phase shift and is then incident internally on the cryodeposit-vacuum interface at point C at the angle β_j. Some fraction of this internally incident ray is transmitted and scattered by the cryodeposit-vacuum interface into an S_j family of rays. The S_j family has an infinite number of scattered rays and a refracted component, ray CL, which lies at the angle θ_j. Angles θ_j and β_j are related by Snell's law. It should be noted that the S_s family of rays shown in Fig. 9 is not due to an arbitrary scattered ray in the t distribution like the S_j families are but is due to the refracted component of the t distribution.

An analysis of the various interference possibilities between the rays shown in Fig. 9 has been made,[3] and it is found that the observed scattering interference patterns are due to interference between rays such as AD and $ABCL$.** Ray AD

** In this analysis, the effects of the scattered rays in the S_j family are assumed to be negligible since these rays correspond to the scattering of a scattered ray.

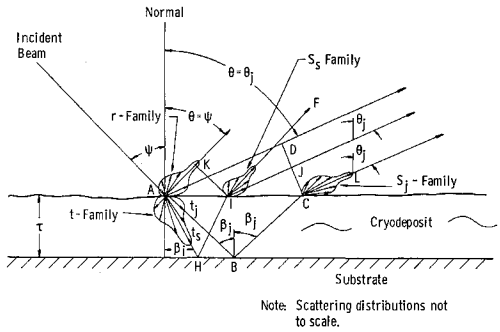

Fig. 9 Sketch of scattering interference model.

is any nonspecular ray in the r family which leaves the cryodeposit surface in the same angular direction θ_j as the refracted component CL of an S_j family. Because waves in the r family and the S_j family have both undergone 180° phase shifts, ray $ABCL$ will constructively interfere with ray AD if their optical path lengths differ by an integer number m of wavelengths. Mathematically, this condition is expressed as $nl_{ABC} - l_{AD} = m\lambda$. The geometric lengths l_{ABC} and l_{AD} are easily related to the cryodeposit thickness τ by inspection of Fig. 9 and use of Snell's law. This allows the development of the following expression for cryodeposit thickness τ in terms of the angular locations θ_j of the interference peaks,

$$\tau = m\lambda/[2n(1 - \sin^2\theta_j/n^2)^{1/2}] \quad (4)$$

This equation expresses the criterion for constructive interference between rays such as AD and $ABCL$ when m takes on integer values. These two rays would destructively interfere for half-integer values of m.

Since t_j is an arbitrary scattered ray in the t family, there is an infinite number of scattered rays in that family which are specularly reflected from the substrate and then scattered by the cryodeposit-vacuum interface to produce S_j families. For a given cryodeposit thickness, the refracted components of some of these S_j families would interfere with particular r-family rays to produce an interference pattern such as shown in Fig. 8. Peaks occur because of constructive interference at discrete angles $\theta_1, \theta_2, \theta_3, \ldots, \theta_j, \ldots$ when Eq. (4) can be simultaneously satisfied by

$$m = m_1 - j + 1 \text{ for } \theta_j, j = 1, 2, 3, \ldots \quad (5)$$

Valleys are produced by destructive interference at the intermediate angles corresponding to half-integer values of m. The integer values of m simultaneously satisfying Eq. (4) are not known in advance. However, for a set of interference peaks (i.e., a set of θ_j's), unique values can easily be found for the m's as follows. In Eq. (5), $m_1 - i + 1$ is the order of the ith observed peak, which occurs at θ_i, and $m_1 - k + 1$ is of the order of the kth observed peak, which occurs at θ_k with $\theta_k > \theta_i$ and $k > i$. Substituting these values into Eq. (4) yields the following relation for $m_1 - i + 1$,

$$m_1 - i + 1 = \frac{(k - i)}{[1 - (1 - \sin^2\theta_k/n^2)^{1/2}/(1 - \sin^2\theta_i/n^2)^{1/2}]} \quad (6)$$

The closest integer to the value of $m_1 - i + 1$ obtained from Eq. (6) is the order of the interference peak occurring at θ_i. The remaining integer values of m associated with the interference peaks occurring at the other θ_j's are then easily found from Eq. (5).

Equations (5) and (6) have been used to determine the integer values of the m's for the interference peaks seen in Fig. 8. These values are given at the top of the associated peaks. Once the m's have been determined, it is possible to calculate the thickness τ of the cryodeposit from Eq. (4) using the m value associated with the ith peak observed at θ_i.

This has been done for the results shown in Fig. 8 and the value of τ obtained for each of the scattering interference patterns is indicated inside the border of the associated graph. It is seen that the values of τ calculated from Eq. (4) are in excellent agreement with the 13.37-μ thickness measured by the standard optical technique described earlier. Once the cryodeposit thickness has been calculated from the results for the ith interference peak, the angular locations θ_j of the remaining interference peaks can be theoretically predicted by use of Eq. (4). These theoretical values for the θ_j's are in excellent agreement with the experimentally observed ones seen on the graphs in Fig. 8.

Conclusions

From the results presented for the angular distribution of visible and near IR radiant flux reflected from CO_2 cryodeposits formed on polished copper and black epoxy paint substrates, the following conclusions may be drawn:

1) The presence of a CO_2 cryodeposit on either a polished copper or black paint substrate causes visible and near IR irradiance to be reflected more diffusely. The specular peak in the reflected flux distribution diminishes with increasing CO_2 cryodeposit thickness until, at a deposit thickness of about 70 μ, it disappears completely for incidence angles less than 70°. For a CO_2 deposit thickness of 270 μ, the angular distribution of the reflected flux is approximately cosine. However, the radiant flux reflected into directions lying within the quadrant of incidence is somewhat larger than the flux reflected into directions lying within the quadrant of specular reflection. Thus, CO_2 cryodeposits scatter more in the backward direction than in the forward.

2) Off-specular peaks are observed in the angular distributions of the visible and near IR radiant flux reflected from CO_2 cryodeposits formed on a black epoxy paint substrate. These peaks occur for irradiance incidence angles equal or greater than 50°, and their angular displacement from the specular direction is a function of incidence angle and cryodeposit thickness and deposition rate. Off-specular peaks are also observed in the distribution results for thick CO_2 cryodeposits formed on polished copper.

3) Interference peaks occur in the angular distributions of radiant flux reflected from relatively thin CO_2 cryodeposits formed on polished copper. A simple theoretical model explaining the existence of these interference patterns is given. It shows that the patterns are a result of interference which is generated by scattering of the incident radiation at the vacuum-cryodeposit interface. Based on this theoretical model, a simple equation is derived for calculating cryodeposit thickness from the scattering interference measurements. Deposit thicknesses obtained by this method are in excellent agreement with the deposit thicknesses determined using optical techniques commonly employed for measuring the thickness of thin films.

In regard to the complications introduced in thermal-vacuum space simulation tests by CO_2 cryodeposits forming on the cryogenically-cooled black chamber walls, the results reported herein indicate that 1) The presence of CO_2 cryodeposits on black space chamber walls will cause the irradiance from the solar simulator to be reflected more diffusely and 2) If the cryodeposit thickness is less than 70 μ, the effect of both diffuse and specular wall reflections on thermal balance test results should be considered. When the cryodeposit thickness is greater than about 150 μ, the reflection of solar simulator irradiance from the black chamber walls can be treated as being diffuse.

References

[1] Wood, B. E. and Smith, A. M., "Spectral Reflectance of Water and Carbon Dioxide Cryodeposits from 0.36 to 1.15 μ," *AIAA Journal*, Vol. 6, No. 7, July 1968, pp. 1362–1367.

[2] McCullough, B. A., Wood, B. E., and Dawson, J. P., "Thermal Radiative Properties of Carbon Dioxide Cryodeposits from 0.5 to 1.1 Microns," TR-65-94 (AD468632), Aug. 1965, Arnold Engineering Development Center, Arnold Air Force Station, Tenn.

[3] Tempelmeyer, K. E., Wood, B. E., and Mills, D. W., Jr., "In Situ Measurement of Thickness and Other Properties of Carbon Dioxide Cryodeposits by Optical Techniques," TR-67-226 (AD662869), Dec. 1967, Arnold Engineering Development Center, Arnold Air Force Station, Tenn.

[4] Tempelmeyer, K. E. and Mills, D. W., Jr., "Refractive Index of Carbon Dioxide Cryodeposit," *Journal of Applied Physics*, Vol. 39, No. 6, May 1968, pp. 2968–2969.

[5] Tempelmeyer, K. E., Müller, P. R., and Smith, A. M., "Angular Distribution of Radiation Reflected from Carbon Dioxide Cryodeposits Formed on 77°K Surfaces," TR-68-46 (AD668432), April 1968, Arnold Engineering Development Center, Arnold Air Force Station, Tenn.

[6] Pliskin, W. A. and Conrad, E. E., "Nondestructive Determination of Thickness and Refractive Index of Transparent Films," *IBM Journal*, Vol. 8, No. 1, Jan. 1964, pp. 43–51.

[7] Dunn, S. T., Richmond, J. C., and Parmer, J. F., "Survey of Infrared Measurement Techniques and Computational Methods in Radiant Heat Transfer," *Journal of Spacecraft and Rockets*, Vol. 3, No. 7, July 1966, pp. 961–975.

[8] Torrance, K. E. and Sparrow, E. M., "Off-Specular Peaks in the Directional Distribution of Reflected Thermal Radiation," *Journal of Heat Transfer*, Vol. 88, Ser. C, No. 2, May 1966, pp. 223–230.

[9] Dunkle, R. V., "Thermal Radiation Characteristics of Surfaces," *Theory and Fundamental Research in Heat Transfer*, Pergamon, New York, 1963, p. 17.